Published in final edited form as:

Nat Immunol. 2016 May ; 17(5): 556–564. doi:10.1038/ni.3390.

Protein phosphatase 2A is requisite for the function of regulatory T cells

Sokratis A. Apostolidis, **Noé Rodríguez-Rodríguez**, **Abel Suárez-Fueyo**, **Nikolina Dioufa**, **Esra Ozcan**, **José C. Crispín**, **Maria G. Tsokos**, and **George C. Tsokos**

Department of Medicine, Beth Israel Deaconess Medical Center, Harvard Medical School, Boston, Massachusetts, USA

Abstract

Immune homeostasis depends on the proper function of regulatory T (T_{reg}) cells. Compromised T_{reg} cell suppressive activity leads to autoimmune disease, graft rejection and promotes anti-tumor immunity. Here we report the previously unrecognized requirement of the serine/threonine phosphatase Protein Phosphatase 2A (PP2A) for the function of T_{reg} cells. T_{reg} cells exhibited high PP2A activity and T_{reg} cell-specific ablation of the PP2A complex resulted in a severe, multi-organ, lymphoproliferative autoimmune disorder. Mass spectrometric analysis revealed that PP2A associates with components of the mTOR pathway and suppresses mTORC1 activity. In the absence of PP2A, T_{reg} cells altered their metabolic and cytokine profile and were unable to suppress effector immune responses. Therefore, PP2A is requisite for the function of T_{reg} cells and the prevention of autoimmunity.

Introduction

Immunological tolerance is achieved through the elimination of self-antigen specific T cell clones generated in the thymus and through the active suppression of autoreactive T cell thymic escapees in the periphery by regulatory T cells (T_{reg} cells)[1]. T_{reg} cells express the signature transcription factor Foxp3 and have a distinct metabolic, proliferation and cytokine profile[2,3]. These characteristics are inherent in their ability to suppress allowing them to maintain immune homeostasis and loss of T_{reg} cell function leads invariably to autoimmunity in mice[4] and humans[5].

Protein phosphatase 2A (PP2A) is a highly conserved serine/threonine phosphatase that is the assembly product of three distinct subunits - termed scaffold A, regulatory B and catalytic C - into a trimolecular complex[6,7]. The heterodimer of the scaffold A and the catalytic C subunit ($PP2A_A/PP2A_C$) forms the PP2A core enzyme that associates with one

Correspondence should be addressed to G.C.T. (; Email: gtsokos@bidmc.harvard.edu)

Author contributions

S.A.A. designed, performed and analyzed experiments and wrote the manuscript; N.R.R., A.S.F., N.D., E.O. and J.C.C. performed and analyzed experiments; M.T. analyzed the histopathology samples; G.C.T designed the overall study, analyzed the data and wrote the manuscript.

The authors have no competing financial interests to declare.

of the regulatory B subunits. The PP2A holocomplex regulates key cellular processes, such as cell cycle progression, apoptosis, cellular metabolism and migration[7]. PP2A is involved in the development of cancer[8], neurodegenerative diseases[9] and systemic lupus erythematosus (SLE)[10]. In SLE, PP2A has been implicated in the regulation of the production of interleukin 2 (IL-2) and IL-17 by $CD4^+$ T cells and in the control of T cell apoptosis induced upon IL-2 deprivation[10,11]. Furthermore, PP2A plays a central role in MyD88-dependent endotoxin tolerance[12], T cell-mediated anti-tumor responses[13] and in the termination of IRF3-dependent type I interferon signaling after viral infection[14].

T_{reg} cells depend on several activating signals including the T cell antigen receptor (TCR), CD28 and IL-2 signaling pathways for their survival and function. Specifically, T_{reg} cells are agonist-selected by high-affinity TCR ligands in the thymus[15] and continuous TCR engagement is required for their maintenance in the periphery[16]. Loss of CD28 (ref. 17) or the IL-2–IL-2 receptor[18,19] signaling results in profound T_{reg} cell impairment and autoimmunity. Paradoxically, while T_{reg} cell function needs the constant presence of these activating signals, T_{reg} cells display diminished activity of several key downstream signaling pathways including the mechanistic target of rapamycin (mTOR)[3,20] and the phosphatidylinositol-3-OH kinase (PI(3)K)-AKT[21,22] pathway compared to other antigen-experienced T cells. Therefore, T_{reg} cells utilize additional negative regulators compared to conventional T (T_{conv}) cells to rewire these downstream signaling relays. Previous reports have established that negative regulation of the PI(3)K-AKT pathway by the Nrp1-SEMA4a axis[23] and of the mTORC2 pathway by PTEN[22] in T_{reg} cells is indispensable for the maintenance of their suppressive function. However, very little is known about how T_{reg} cells control the mTORC1 complex in a cell-intrinsic manner and whether this regulation is integral for their function.

In this report, we demonstrate that the serine-threonine phosphatase PP2A controls the activity of the mTORC1 complex in T_{reg} cells allowing them to maintain a metabolic and cytokine profile that is essential for their suppressive function. T_{reg} cell-specific loss of PP2A causes a severe lymphoproliferative and autoimmune disorder with spontaneous immune system activation and autoantibody production.

Results

Ablation of PP2A in T_{reg} cells leads to autoimmunity

The PP2A holoenzyme structurally consists of three different proteins: the catalytic C subunit ($PP2A_C$), the scaffold A subunit ($PP2A_A$) and the regulatory B subunit ($PP2A_B$)[6,7]. When we compared the catalytic activity of the PP2A complex in T_{reg} and T_{conv} cells, T_{reg} cells displayed increased PP2A activity (Supplementary Fig. 1a). The nascent catalytic $PP2A_C$ subunit -encoded by two different isoforms Cα and Cβ is produced in an inactive state and undergoes an activation process that is coupled to its incorporation with the scaffold $PP2A_A$ subunit into the heterodimeric $PP2A_A$-$PP2A_C$ core[24–26]. The absence of $PP2A_A$ prevents the maturation of the catalytic subunit into its active state and the PP2A catalytic activity is impaired[24]. The scaffold $PP2A_A$ subunit is also encoded by two isoforms, Aα and Aβ with gene names *Ppp2r1a* and *Ppp2r1b* respectively, with the former being the dominant in primary and secondary lymphoid organs[27] as well as in isolated $CD4^+$

T cells (Supplementary Fig. 1b). Accordingly, to study the role of PP2A in T_{reg} cell function, we deleted the dominant α isoform *(Ppp2r1a*) of the scaffold $PP2A_A$ subunit in a T_{reg} cell-specific manner by crossing *Foxp3*$^{YFP\text{-}cre}$ mice with *Ppp2r1a*$^{flox/flox}$ mice to generate *Foxp3*$^{YFP\text{-}cre}$*Ppp2r1a*$^{flox/flox}$ (termed here $PP2A^{flox}$) and *Foxp3*$^{YFP\text{-}cre}$*Ppp2r1a*$^{flox/+}$ or *Foxp3*$^{YFP\text{-}cre}$*Ppp2r1a*$^{+/+}$ (both termed here $PP2A^{wt}$ because we did not appreciate any haploinsufficiency of *Ppp2r1a* in the T_{reg} cell population).

By the age of 10–14 weeks, the $PP2A^{flox}$ mice developed spontaneously severe, progressive, multi-organ autoimmunity characterized by wasting, dermatitis, scaly tails and ears, eyelid crusting and in some occasions overt skin rash and ulcerations (Fig. 1a and Supplementary Fig. 1c–f). The clinical picture displayed similarities to the scurfy (*sf*) phenotype, where the *sf* mice harbor a spontaneous mutation mapped to the *Foxp3* gene[28] and develop early-onset, multi-organ autoimmunity. Upon macroscopic examination of the organs, it was evident that the $PP2A^{flox}$ mice suffered a lymphoproliferative syndrome with secondary lymphoid organ enlargement (Fig. 1b and Supplementary Fig. 1g and h). Histologic examination of the $PP2A^{flox}$ mice revealed extensive inflammatory infiltrates in the lungs, stomach, pancreas, salivary glands and the skin (Fig. 1c and Supplementary Fig. 1d). In the lungs, extensive lymphocytic infiltrates were appreciated, especially in the perivascular and peribronchial areas. This cellular infiltration was accompanied by parenchymal consolidation and thickening of the alveolar walls. In the skin, dermal thickening and epidermal hyperplasia with spongiosis, hyperkeratosis and parakeratosis were noted. Lymphoid and polymorphonuclear aggregates in the dermis were abundant and occasionally extended into the epidermis. Focal micro-abscess formation in the stratum corneum and ulceration were also observed. Periductal and perivascular lymphocytic infiltrates were evident in the pancreas and salivary glands and around the pancreatic islets of the $PP2A^{flox}$ mice. In the stomach, inflammatory aggregates, composed of lymphocytes, polymorphonuclear leukocytes and eosinophils, were observed in the submucosa protruding into the adjacent mucosal layer.

The spontaneous autoimmune phenotype of the $PP2A^{flox}$ mice prompted us to examine the status of their immune system compared to their wild-type littermates. We observed increased T cell activation in both $CD4^+$ and $CD8^+$ T cells, as evidenced by the presence of increased percentages of $CD44^+CD62L^-CD4^+$, $CD44^+CD62L^-CD8^+$ and $CD44^+CD62L^+CD8^+$ T cells in the spleen, peripheral and mesenteric lymph nodes (Fig. 2a). When stimulated *ex vivo*, $CD4^+$ T cells of the $PP2A^{flox}$ mice produced significantly higher amounts of IL-17 and IL-2 and the $CD8^+$ T cells of the $PP2A^{flox}$ mice produced increased amounts of interferon-γ (IFN-γ) and tumor necrosis factor (TNF) (Fig. 2b). EdU incorporation by $CD4^+$ T cells was accentuated in $PP2A^{flox}$ mice demonstrating their higher proliferative state (Supplementary Fig. 2). $PP2A^{flox}$ mice demonstrated higher concentrations of all immunoglobulin classes (IgM, IgG, IgE and IgA) (Fig. 2c). Congruent with these findings was the increased percentage of T follicular helper ($CD3^+CD4^+PD1^+CXCR5^+$) cells and germinal center B ($CD19^+FAS^+GL7^+$) cells in the spleens of the $PP2A^{flox}$ mice (Fig. 2d). To determine whether $PP2A^{flox}$ mice produced autoantibodies, we used an autoantigen array that interrogates 128 known autoantigens. We detected the presence of IgG autoantibodies for 76 autoantigens that included both tissue-restricted and lupus-associated nuclear autoantigens (Fig. 2e). These results indicated that

the dominant tolerance exerted by the T_{reg} cells was lost in the $PP2A^{flox}$ mice. Additionally, the absence of any signs of autoimmunity or spontaneous immune system activation in the female *Foxp3*$^{YFP\text{-}cre/+}$*Ppp2r1a*$^{flox/flox}$ mice (data not shown), where approximately half of the T_{reg} cell population is PP2A sufficient, further suggested that the loss of T_{reg} cell-mediated suppression is responsible for the phenotype recorded in the $PP2A^{flox}$ mice.

Ceramide accumulation activates PP2A in T_{reg} cells

Our results suggested that PP2A is necessary for T_{reg} cells to maintain their suppressive function. Thus, we investigated the mechanisms that regulate the activity of the PP2A complex in T_{reg} cells. Whereas the abundance of the catalytic $PP2A_C$ subunit is remarkably stable in a particular cell state[29], its activity is controlled through post-translational modifications at its carboxy-terminal tail[30]. Specifically, phosphorylation of the Y307 residue at the C-terminal end of the $PP2A_C$ protein results in PP2A inactivation[30,31]. When we activated $CD4^+$ T_{conv} cells with anti-CD3 plus anti-CD28, we detected $PP2A_C$ (Y307) phosphorylation within 24 h of activation (Fig. 3a). However, we did not detect the same behavior in T_{reg} cells, which retained low amounts of Y307 phosphorylation after CD3 plus CD28 stimulation (Fig. 3b and Supplementary Fig. 3a) consistent with their increased PP2A activity (Supplementary Fig. 1a). Notably, the total amount of the $PP2A_C$ subunit in T_{reg} cells was similar to T_{conv} cells both before and after CD3 plus CD28 stimulation (Fig. 3c).

The $PP2A_C$ (Y307) phosphorylation is under the control of the ceramide-SET pathway. The SET protein (originally named *I^2PP2A* for inhibitor 2 of PP2A) has been identified as an inducer of Y307 phosphorylation and thus an inhibitor of PP2A activity[32–34]. In $CD4^+$ T cells, we found that *Set* is a highly TCR-responsive gene with kinetics of induction that paralleled those of the Y307 phosphorylation of $PP2A_C$ (p-$PP2A_C$) following CD3 plus CD28 stimulation of $CD4^+$ T cells (Fig. 3d). Lentiviral infection of $CD4^+$ T cells with a *Set*-expressing vector and knockdown experiments with a *Set*-specific shRNA promoted and decreased p-$PP2A_C$ (Y307) respectively after anti-CD3 plus anti-CD28 stimulation (Fig. 3e and Supplementary Fig. 3b), indicating that SET is responsible for the Y307 phosphorylation of $PP2A_C$ upon activation of $CD4^+$ T cells. However, T_{reg} and T_{conv} cells exhibited similar induction of SET upon stimulation with anti-CD3 plus anti-CD28 (Fig. 3f). Thus, to investigate the cause of differential Y307 phosphorylation of $PP2A_C$ in T_{reg} and T_{conv} cells, we turned our focus to ceramide, the upstream regulator of the ceramide-SET pathway. Specifically, the SET-mediated induction of p-$PP2A_C$ (Y307) can be abolished by an increase in the intracellular abundance of ceramide, because ceramide interacts with SET and constraints its inhibitory action on the PP2A complex, thus representing an important endogenous PP2A activator[35–37]. Indeed, treatment of T cells with sphingomyelinase (SMase), which increases endogenous ceramide content (Fig. 4a), reduced the association of the SET protein with $PP2A_C$ (Supplementary Fig. 3c). Accordingly, SMase treatment of activated $CD4^+$ T cells decreased the Y307 phosphorylation of $PP2A_C$ (Fig. 4b and Supplementary Fig. 3d). To quantify the abundance of the ceramide species present in T_{reg} and T_{conv} $CD4^+$ cells, we used high performance liquid chromatography coupled with electrospray ionization tandem mass spectrometry (ESI-MS/MS) and found that T_{reg} cells display higher amounts of several ceramide species compared to T_{conv} cells (Fig. 4c). Flow

cytometry for total ceramide content corroborated these results at the single-cell level (Fig. 4d).

We subsequently explored the mechanism that leads to T_{reg}-specific accumulation of intracellular ceramide. Sphingomyelin synthase 1 (gene name *Sgms1*) is an enzyme of the sphingolipid metabolism pathway that has been previously shown to be part of the T_{reg} cell signature[38] and underexpressed in T_{reg} cells. *Sgms1* catalyzes the conversion of ceramide and phosphatidylcholine to diacylglycerol and sphingomyelin. Low amounts of *Sgms1* result in accumulation of ceramide intracellularly[39,40]. Chromatin immunoprecipitation (ChIP) experiments demonstrated that the *Sgms1* gene is a direct FoxP3 target (Fig. 4e) and retroviral overexpression of *FOXP3* in Jurkat T cells decreased the expression of *SGMS1* at the mRNA and protein level (Supplementary Fig. 4a and b) in agreement with previous data[41]. Lentiviral infection of murine $CD4^+$ T cells with an *Sgms1*-expressing vector reduced, accordingly, the intracellular abundance of ceramide (Fig. 4f). Therefore, T_{reg} cells have a cell-intrinsic mechanism to maintain increased PP2A activity. Foxp3-mediated suppression of S*gms1* results in accumulation of ceramide in T_{reg} cells that leads to activation of the PP2A complex.

PP2A inhibits mTORC1 in T_{reg} cells

To delineate the specific contribution of ceramide-mediated PP2A activation in T_{reg} cell function, we activated the PP2A complex in Jurkat T cells using SMase. $PP2A_C$ immunoprecipitation was performed and bands that represented increased association with $PP2A_C$ after SMase treatment were subjected to mass spectrometry (Supplementary Fig. 5a). The results were controlled for false discovery rate and any hits that were identified in the bands of the same height of the IgG fraction were subtracted. We identified 269 unique proteins associated with $PP2A_C$ after ceramide activation (Supplementary Table 1). Ingenuity Pathway Analysis (IPA) revealed that the major associated pathway was the mTOR pathway (Supplementary Fig. 5b). We verified the association of $PP2A_C$ after SMase treatment with the key component of the mTORC1 complex Raptor (Supplementary Fig. 5c) that represented one of the identified proteins. To determine the specific effect that PP2A activation has on the mTOR signaling pathway, we examined the activity of the mTORC1 complex by checking the phosphorylation of the ribosomal S6 protein (p-S6), of the mTORC2 complex by checking the S473 phosphorylation of Akt ($p\text{-}Akt^{S473}$) and of the PI(3)K by checking the T308 phosphorylation of Akt ($p\text{-}Akt^{T308}$). Ceramide activation had a unique effect on mTORC1 complex activity and a negligible effect on mTORC2 and PI(3)K (Fig. 5a). Similar results were obtained when we used isolated primary murine $CD4^+$ T cells (Fig. 5b). Specifically, SMase treatment of the $CD4^+$ T cells reduced significantly the phosphorylation of S6 and pharmacologic inhibition of PP2A with okadaic acid increased p-S6. Importantly, the SMase-induced decrease of p-S6 was completely abrogated when PP2A was inhibited with okadaic acid. We observed a slight decrease in $p\text{-}Akt^{S473}$ upon treatment of murine $CD4^+$ T cells with SMase and no change in $p\text{-}Akt^{T308}$. Flow cytometric analysis of p-S6 directly *ex vivo* in $PP2A^{wt}$ and $PP2A^{flox}$ mice showed that $PP2A^{flox}$ T_{reg} cells have significantly increased phosphorylation of S6 (Fig. 5c).

mTOR is centrally involved in the regulation of several key cellular processes, including nutrient sensing, cell proliferation and metabolism[42]. In T cells, mTOR additionally exerts control over cytokine production and T cell differentiation[3]. The increased activity of the mTORC1 complex in PP2A^{flox} T_{reg} cells (Fig. 5c), coupled with the loss of T_{reg} cell-mediated tolerance in the PP2A^{flox} mice, prompted us to examine the phenotypic characteristics of PP2A^{flox} and PP2A^{wt} T_{reg} cells. Specifically, we quantified the glycolytic and mitochondrial respiratory capacity using a Seahorse XF24 instrument. PP2A^{flox} T_{reg} cells had significantly elevated baseline and maximum glycolytic rate (Fig. 6a). Similarly, PP2A^{flox} T_{reg} cells displayed increased oxidative phosphorylation rate both at baseline and at maximum capacity (Fig. 6b). The level of augmented glycolytic and oxidative phosphorylation rate of the PP2A^{flox} T_{reg} cells was comparable or higher than the corresponding level of glycolytic and oxidative phosphorylation rate of wild-type T_{conv} cells before and after CD3 plus CD28 stimulation (Supplementary Fig. 6a). *In vivo* determination of the proliferation rate of T_{reg} cells was done with EdU injected i.p. in PP2A^{wt} and PP2A^{flox} mice. PP2A^{flox} T_{reg} cells displayed increased EdU incorporation indicating that they proliferate more than the PP2A^{wt} T_{reg} cells (Fig. 6c). These results were congruent with our observation of an increased percentage of T_{reg} cells in the spleens, peripheral and mesenteric lymph nodes of the PP2A^{flox} mice (Fig. 6d). In addition, *ex vivo* stimulation resulted in increased production of IL-2 and IL-17 in PP2A^{flox} T_{reg} cells compared to PP2A^{wt} T_{reg} cells (Fig. 6e). PP2A^{flox} T_{reg} cells exhibited similar expression of the surface markers CD25, CTLA-4, PD-1, LAP, CD73, GITR and FR-4 (Fig. 6f and Supplementary Fig. 6b) to PP2A^{wt} T_{reg} cells, but increased expression of the large neutral amino acid transporter (LAT1) CD98 (Fig. 6g) that depends on mTORC1 activity[43]. PP2A^{flox} T_{reg} cells did not suppress to the same extent as the PP2A^{wt} T_{reg} cells the proliferation of effector T cells in an *in vitro* suppression assay (Fig. 6h).

To determine the functional importance of the deregulation of the mTORC1 pathway in PP2A-deficient T_{reg} cells, we assessed the ability of the mTORC1 inhibitor rapamycin to reverse the abnormal phenotype of the PP2A^{flox} T_{reg} cells. Rapamycin treatment *in vitro* of PP2A^{flox} T_{reg} cells reduced the production of IL-2 and IL17 (Fig. 7a). In addition, rapamycin normalized their increased glycolytic and oxidative phosphorylation rate to the levels of the PP2A^{wt} T_{reg} cells (Fig. 7b). *In vivo* administration of rapamycin (3 mg/kg i.p. every other day[44]) to PP2A^{flox} mice reduced the leukocyte infiltration in the affected peripheral tissues (Fig. 7c). Rapamycin administration also normalized the proportion and numbers of effector $CD4^+$ and $CD8^+$ T cells in PP2A^{flox} mice such that those were comparable to PP2A^{wt} mice (Supplementary Fig. 7a and b). T_{reg} cells from treated mice displayed decreased p-S6 (Fig. 7d), indicating decreased mTOR signaling. This inhibition was also evident by a reduction of the surface expression of the mTOR-dependent amino acid transporter CD98 (Fig. 7e). Importantly, T_{reg} cells from rapamycin-treated PP2A^{flox} mice suppressed effectively the proliferation of *in vitro* activated wild-type naïve $CD4^+$ T cells (Fig. 7f). In addition, rapamycin treatment decreased the proportion of follicular helper T cells and germinal center B cells in PP2A^{flox} mice (Supplementary Fig. 7c and d). We conclude that PP2A-mediated inhibition of mTORC1 is necessary for the suppressive function of T_{reg} cells and treatment of PP2A^{flox} T_{reg} cells with rapamycin *in vitro* and *in vivo* re-establishes their suppressive function, metabolic and cytokine profile.

Discussion

With the exception of PTEN, the role of intracellular phosphatases in the control of T_{reg} cell function is poorly understood. In this communication, we report that T_{reg} cells require PP2A, an evolutionary conserved serine/threonine phosphatase, to suppress effector immune cell function. Mass spectrometric, pathway enrichment and intracellular signaling analysis revealed that PP2A operates though inhibition of the mTORC1 pathway. Previous studies have shown that increased activity of the mTOR pathway negatively impacts T_{reg} cell generation and function[20,22,45,46]. Interestingly, abrogation of the mTORC1 complex in T_{reg} cells in *Foxp3*$^{YFP\text{-}cre}$*Raptor*$^{flox/flox}$ mice[43] also disrupts T_{reg} cell function, indicating that fine regulation of the activity of this pathway rather than its complete absence is the determining factor for T_{reg} cell operational fitness. Ceramide-mediated activation of PP2A provides T_{reg} cells with required phosphatase activity to control mTORC1 and establish their tolerogenic metabolic and cytokine profile.

Foxp3, the main transcriptional regulator of T_{reg} cells, utilizes the pre-existent transcriptional landscape of the activated $CD4^+$ T cell to establish T_{reg} cell function[47] acting largely as a repressor[41]. However, our understanding of the translation of the Foxp3-dependent epigenetic regulation to intracellular signaling events is limited. Ceramides have recently been recognized as important intracellular bioactive metabolites and second messengers[48]. A major effect of ceramide is the activation of the PP2A complex[35–37]. SGMS1, an enzyme of the sphingolipid metabolism, regulates the ceramide amount of the cell and has consistently been recognized in microarray studies as one of the main genes repressed in T_{reg} cells[38]. Here we show that *Sgms1* is a direct Foxp3 target and, thus, we provide a link between Foxp3 function and PP2A-mediated signaling effects.

PP2A is implicated in the regulation of key intracellular signaling pathways, including but not limited to the AKT, MAPK and JAK-STAT pathways[7,8]. The relative importance of each of these associations depends on the cellular type and the interrogated biologic response. Thus, it was crucial in our system to define the main downstream signaling events following PP2A activation. Our experiments highlight the importance of the interaction between PP2A and the mTOR pathway in T_{reg} cells. Given the well-established association of PP2A with AKT[49] and AKT with T_{reg} cells[21–23,50], we investigated independently the effect of PP2A activation on AKT phosphorylation. We found that ceramide-mediated activation of PP2A has minimal effect on the mTORC2-dependent Akt^{S473} phosphorylation and no effect on the PI(3)K-mediated Akt^{T308} phosphorylation. We concluded that activation of PP2A in T_{reg} cells in a ceramide-dependent manner targets mainly the mTORC1 signaling.

In this report, we have provided evidence that T_{reg} cell function depends on the presence of PP2A and in its absence mice develop profound lymphoproliferation and autoimmunity. We propose that therapeutic enhancement of PP2A activity in T_{reg} cells should mitigate autoimmunity and transplant rejection and inhibition of the PP2A complex in T_{reg} cells should compromise their function and promote the fight of the immune system against cancer.

Online Methods

Mice

C57BL/6J (strain: 000664), Foxp3-IRES-eGFP (strain: 018628) and CD45.1 (strain: 002014) mice were purchased from the Jackson Laboratory. To generate PP2A^{flox}, *Ppp2r1a*$^{flox/flox}$ mice[51] (strain: 017441, Jackson Laboratory, FVB background) were back-crossed for at least 7 generations into C57BL/6J mice. Subsequently they were bred with *Foxp3*$^{YFP\text{-}cre}$ mice[52] (strain: 016959, Jackson Laboratory) to generate *Foxp3*$^{YFP\text{-}cre}$*Ppp2r1a*$^{flox/flox}$ mice. Both age- and sex-matched male and female mice at the age of 10–14 weeks (unless indicated otherwise in the figure legend) were used for experiments. For the *in vivo* treatment experiments with rapamycin, 3mg/kg of rapamycin was administrated by i.p. injection every other day as described previously[44] for 4–5 weeks. Blood was collected before the first administration and weekly afterwards to assess lymphocyte activation. All mice were bred and housed in a specific pathogen-free environment in a barrier facility in accordance to the Beth Israel Deaconess Medical Center Institutional Animal Care and Use Committee (IACUC).

Antibodies and reagents

Antibodies against PP2A$_C$ (clone: 1D6, Millipore), phospho-PP2A$_C$ (Y307, clone: E155, Epitomics), SET (clone: EPR12972(B), Abcam), Raptor (clone: 24C12, Cell Signaling), Foxp3 (clone: 150D, BioLegend and clone: D6O8R, Cell Signaling), Ceramide (clone MID 15B4, Sigma-Aldrich), phospho-S6 (Pacific Blue conjugate, clone: D57.2.2E, Cell Signaling), phospho-Akt (Ser473, Alexa Fluor 647 conjugate, clone: D9E, Cell Signaling), phospho-Akt (T308, Alexa Fluor 488 conjugate, clone: C31E5E, Cell Signaling) and SGMS1 (Thermo Scientific, cat# PA1-12761) were used for immunoblot, immunoprecipitation, ChIP and flow cytometry experiments. Staining for phospho-flow experiments was performed using the Beckman Coulter PerFix Expose kit (cat#: B26976). All flow cytometry antibodies for T cell and B cell sorting and cytokine production (CD3, clone: 145-2C11; CD4, clone: GK1.5; CD8, clone: 53-6.7; CD44, clone: IM7; CD62L, clone: MEL-14; CD45.1, clone: A20; CXCR5, clone: 2G8; PD1, clone: 29F.1A12; GL7, cat # 114612; FAS, clone: 15A7; CD25, clones: 3C7 and PC61; CTLA4, clone: UC10-4B9; CD73, clone: TY/11.8 LAP, clone: TW7-16B4; GITR, clone: DTA-1; FR4, clones: TH6 and 12A5; CD98, clone: RL388; IL-17, clone: TC11-18H10.1; IL-2, clone: JES6-5H4; IFN-γ, clone: XMG1.2; IL-4, clone: 11B11; TNF, clone: MP6-XT22) were from BioLegend. All antibodies have been validated by their suppliers and references can be found on their website or on the online validation databases Antibodypedia and 1DegreeBio. Antibody dilutions were 1:1000 for immunoblot, immunoprecipitation and ChIP experiments and 1:100 for flow cytometry experiments. Sphingomyelinase (SMase, used at 0.5 units/ml) from *Staphylococcus aureus* (cat#: S8633), Okadaic Acid (cat#: O9381, used at 10 nM) and Rapamycin (cat#: R0395) were from Sigma-Aldrich. ELISAs for murine IgM, IgG, IgE and IgA were from Affymetrix-eBiosciences. For *in vivo* cell proliferation experiments, the Click-iT Plus EdU Alexa Fluor 647 Flow Cytometry Assay Kit (cat#: C10634, Life Technologies) was used per the manufacturer's instructions.

Glycolytic and mitochondrial respiration rate measurement

For metabolic experiments, a Seahorse XF24 instrument was used. FACS sorted FoxP3-eGFP$^+$ or Foxp3-YFP$^+$CD4$^+$ T cells (Fig. 6a and b) and CD4$^+$CD25$^+$ T cells (isolated as described below; Supplementary Fig. 6a) were seeded at a density of 5×10^5 per well. The extracellular acidification rate (ECAR) and the oxygen consumption rate (OCR) for each well were calculated while the cells were subjected to the XF Cell Mito or the XF Glycolytic stress test protocols. The XF Cell Mito and the XF Glycolytic stress test kits were purchased from Seahorse Biosciences.

T cell isolation

T_{reg} cell isolation for immunoblotting, mass-spectrometric and ChIP experiments was performed using the magnetic separation Dynabeads FlowComp Mouse CD4$^+$CD25$^+$ T_{reg} Cells kit (cat#: 11463D) from Life Technologies. For all other experiments, T_{reg} cells were sorted on a FACS-Aria II (Becton, Dickinson) as CD3$^+$CD4$^+$CD25$^+$Foxp3-eGFP$^+$ T cells. Naïve CD4$^+$ T cell isolation was performed with the magnetic separation Naive CD4$^+$ T Cell Isolation kit (cat#: 130-104-453) from Miltenyi Biotech. In all instances, cells were sorted to more than 95% purity.

Mass-spectrometry

Ceramide species were quantified using high performance liquid chromatography – electrospray ionization tandem mass spectrometry (ESI-MS/MS) at the Lipidomics Analytical Core Facility of the Medical University of South Carolina (MUSC), as previously described[53]. 3×10^6 T_{conv} and 3×10^6 T_{reg} cells were analyzed, after lipid extraction, together with internal sphingolipid controls on a Thermo Fisher Scientific triple quadrupole mass spectrometer operating in a multiple reaction monitoring (MRM) positive ionization mode for the quantification of ceramide species.

For $PP2A_C$–interacting proteins, Jurkat T cells were treated with sphingomyelinase (SMase, 0.5 units/ml) or vehicle (50% glycerol in PBS) for 1 h and then lysed for protein immunoprecipitation with a $PP2A_C$-specific antibody (clone: 1D6, Millipore) or a mouse IgG control antibody. Immunoblot was performed under denaturating conditions with the immunoprecipitates separated on two different gels: a 4–12% Bis-Tris gel (NuPage Novex Life Technologies, SDS-PAGE, pH 7.0) with effective range of separation of 2–200 kDa (Supplementary Fig. 5a) and a 3–8% Tris-Acetate gel (NuPage Novex Life Technologies, pH 8.1) with effective range of separation of 36–400 kDa (data not shown). Bands that were differentially represented between the SMase and the vehicle treated groups were subjected to mass spectrometry for identification of $PP2A_C$-interacting proteins after ceramide-mediated PP2A activation. The bands with corresponding height at the IgG control lane were also excised and any identified proteins were excluded. The results were controlled for false discovery rate and the identified proteins were analyzed with Qiagen's Ingenuity Pathway Analysis (IPA) software for the identification of pathway enrichment in the dataset.

Autoantigen microarray

Serum from 10–14 week-old $PP2A^{wt}$ and $PP2A^{flox}$ mice was analyzed for the presence of autoantibodies using the Autoantigen Microarray Super Panel (128 antigen panel) at the

UTSW Genomics and Microarray Core facility. Autoantibodies that were statistically different between the two groups were used to create a row-normalized heatmap analysis with R software.

Code availability

The pathway analysis for the mass spectrometric data in Supplementary Fig. 5b was done with the use of QIAGEN's Ingenuity Pathway Analysis (QIAGEN Redwood City, www.qiagen.com/ingenuity, IPA Winter Release 2014).

R software was used to analyze and generate the results of the autoantigen array, shown in Fig. 2e. "R Development Core Team (2008). R: A language and environment for statistical computing. R Foundation for Statistical Computing, Vienna, Austria. ISBN 3-900051-07-0, URL http://www.R-project.org".

$PP2A_C$ enzymatic activity

$PP2A_C$ enzymatic activity was assessed using the PP2A Immunoprecipitation Phosphatase Assay Kit (cat#: 17-313, Millipore) per the manufacturer's instructions. Briefly, protein extracts were immunoprecipitated with a $PP2A_C$-specific antibody (clone: 1D6, Millipore). An appropriate phosphopeptide (amino acid sequence: K-R-pT-I-R-R) was added to the immunoprecipitated immune complexes as a substrate for PP2Ac and samples were incubated at 30 °C in a shaking incubator for 10 min. Supernatants (25 μl) were transferred in a 96-well plate and released phosphate was measured by adding 100 μl malachite green phosphate detection solution in a 15-min colorimetric reaction. Phosphate concentrations were calculated from a standard curve created using serial dilutions of a standard phosphate solution.

In vitro suppression assay

$CD45.1^+CD4^+CD62L^+CD25^-CD44^-$ T cells (1×10^5, T_{eff}) were stained with CFSE (Life Technologies) and cultured for 4 days with $PP2A^{wt}$ or $PP2A^{flox}$ T_{reg} cells in serially decreasing ratios (1:1, 1:2, 1:4, 1:8, only T_{eff} cells) in the presence of 1×10^5 irradiated splenocytes and plate-bound anti-CD3 (2 μg/ml, clone 145-2C11; BioXcell). T_{eff} cell proliferation was assessed with the dilution of the CFSE dye using FACS at the end of the 4-day culture.

Plasmid, retroviral and lentiviral infections

For SET-silencing experiments, the psi-mU6 mCherry-expressing vector was used harboring a SET-specific shRNA or a scrambled control (purchased from Genecopeia). For lentiviral overexpression of SGMS1 and SET, the full coding sequences of murine *Sgms1* and *Set* were cloned from cDNA generated from murine $CD4^+$ T cells using the following primers:

Sgms1-cloning-for 5′-ATCTGGAATTCGCAAGCTGGGGGTACTGAAT-3′

Sgms1-cloning-rev 5′-ATTCGGGATCCCATTCCCTAGTCGGCAGAGC-3′

SET-cloning-for 5′-ATCTGGAATTCCTGTCTCCCGGTCATCTCCC-3′

SET-cloning-rev 5′-ATTCGGGATCCAGGGAGGAAAGGACTGCAAC-3′5′-

They were then incorporated using EcoRI and BamHI restriction enzymes into the pLVX-EF1α-IRES-mCherry Lentiviral Vector (cat#: 631987, Clontech Laboratories) and viral particles were generated in HEK293FT cells using the ViraPower Lentiviral Packaging Mix (cat#: K4975-00, Life Technologies). Viral supernatants were concentrated 100-fold with Lenti-X™ Concentrator (cat#: 631231, Clontech Laboratories). Lentiviral infection of naïve $CD4^+$ T cells was performed 24 h after activation with anti-CD3 plus anti-CD28 (2 μg/ml) using spin-infection during which cells were centrifuged at 900*g* for 90 min at 32 °C in the presence of 6 μg/ml of polybrene. Downstream flow cytometry analysis of the infected cells was performed by gating on $mCherry^+$ T cells.

The MSCV-FOXP3-IRES-Thy1.1 used in the *FOXP3* overexpression experiments was a gift from Anjana Rao[54] (Addgene plasmid # 17443). Viral particles were generated as explained previously, using pCG-GagPol and pVSVg helper plasmids and Jurkats T cells were infected two consecutive times as described above. 24 h after the last infection $Thy1.1^+$ cells were sorted and lysed for RNA and protein extraction. For detection of transcripts encoding for *FOXP3* and *SGMS1* the following primers were used:

hFOXP3-forward 5′-GAGAAGCTGAGTGCCATGC-3′

hFOXP3-reverse 5′-AGCCCTTGTCGGATGATG-3′

hSGMS1-forward 5′-GCGATTGGGGTGCGGAG-3′

hSGMS1-reverse 5′-GCCCATTCAGGGATCGTACA-3′

Chromatin Immunoprecipitation

Chromatin immunoprecipitation experiments were performed with the MAGnify Chromatin Immunoprecipitation System (cat#: 49-2024, Life Technologies) following the manufacturer's instructions. Briefly, 2×10^6 cells were cross-linked with 1% formaldehyde for 10 min at 37 °C. The reaction was stopped with glycine for 5 min, and the samples were lysed and sonicated to obtain 200- to 500-bp fragments. Immunoprecipitation was performed with a Foxp3-specific antibody or an IgG control. Cross-linking was reversed, and DNA was eluted and purified using DNA purification magnetic beads. Enrichment of the murine *Sgms1* genomic sequence in the samples was quantified by real-time quantitative PCR and normalized with the input samples. The primers used were *Sgms1-ChIP-forward:* 5′-TGCTGTGAGGTTTTAAGGGGAA and *Sgms1-ChIP-reverse:* 5′-CTTCATAAGCACAAGACGGGC.

T cell stimulation

T cells were stimulated in complete RPMI 1640 with plate-bound anti-CD3 (2 μg/ml, clone 145-2C11; BioXcell) and anti-CD28 (2 μg/ml, clone 37.51; BioLegend) in flat-bottom 96-well plates. For staining of intracellular cytokines, T cells were stimulated with PMA (50 ng/ml) and Ionomycin (250 ng/ml) for 6 h in the presence of GolgiPlug (BD Biosciences) and stained using the Cytofix/Cytoperm kit from BD Biosciences (cat#: 555028).

Cell lines

The human acute T cell leukemia cell line Jurkat (clone E6-1) was purchased from ATCC (cat#: ATCC TIB-152) and has been tested for mycoplasma by ATCC.

Histology

Formalin-fixed tissues were processed, stained with haematoxylin and eosin (H&E) and evaluated blindly.

The clinical score depicted in Fig. 7c represents the combined inflammation score of the following organs: liver, skin, stomach, salivary glands, lungs and pancreas. The inflammation was scored blindly. No infiltration was scored as 0, some cellular infiltration was scored as 0.5 and clear abundant infiltrates were scored as 1. All the scores were added for each organ to produce the combined clinical score.

Statistical Analysis

Student's two-tailed t-test, two-way analysis of variance (ANOVA) followed by Bonferroni's test and one-way ANOVA followed by Tukey's multiple comparison test were used to calculate statistical significance among groups as indicated in the figure legends. A P value of less than 0.05 was considered statistically significant. Results were expressed as the mean ± s.e.m.

Supplementary Material

Refer to Web version on PubMed Central for supplementary material.

Acknowledgments

We thank C. Terhorst for critical reading of the manuscript, P. Seth for advice on the use of the Seahorse XF24 instrument. We would also like to thank J. Bielawski and J. Pierce from the Medical University of South Carolina for advice and technical assistance on the mass spectrometric studies of ceramide species and A. Rao from the La Jolla Institute for Allergy and Immunology for the kind gift of the MSCV-FOXP3-IRES-Thy1.1 plasmid (initially generated at Harvard Medical School and the University of Colorado at Boulder). This work was supported by the National Institutes of Health (NIH RO1 AI068787 to G.C.T.) and the Arthritis Foundation Postdoctoral Fellowship (to S.A.A.).

References

1. Starr TK, Jameson SC, Hogquist KA. Positive and negative selection of T cells. Annu Rev Immunol. 2003; 21:139–176. [PubMed: 12414722]
2. Josefowicz SZ, Lu LF, Rudensky AY. Regulatory T cells: mechanisms of differentiation and function. Annu Rev Immunol. 2012; 30:531–564. [PubMed: 22224781]
3. Chi H. Regulation and function of mTOR signalling in T cell fate decisions. Nat Rev Immunol. 2012; 12(5):325–338. [PubMed: 22517423]
4. Lyon MF, Peters J, Glenister PH, Ball S, Wright E. The scurfy mouse mutant has previously unrecognized hematological abnormalities and resembles Wiskott-Aldrich syndrome. Proc Natl Acad Sci U S A. 1990; 87(7):2433–2437. [PubMed: 2320565]
5. Bennett CL, et al. The immune dysregulation, polyendocrinopathy, enteropathy, X-linked syndrome (IPEX) is caused by mutations of FOXP3. Nat Genet. 2001; 27(1):20–21. [PubMed: 11137993]
6. Xu Y, et al. Structure of the protein phosphatase 2A holoenzyme. Cell. 2006; 127(6):1239–1251. [PubMed: 17174897]

7. Shi Y. Serine/threonine phosphatases: mechanism through structure. Cell. 2009; 139(3):468–484. [PubMed: 19879837]
8. Mumby M. PP2A: unveiling a reluctant tumor suppressor. Cell. 2007; 130(1):21–24. [PubMed: 17632053]
9. Sontag JM, Sontag E. Protein phosphatase 2A dysfunction in Alzheimer's disease. Front Mol Neurosci. 2014; 7:16. [PubMed: 24653673]
10. Tsokos GC. Systemic lupus erythematosus. N Engl J Med. 2011; 365(22):2110–2121. [PubMed: 22129255]
11. Katsiari CG, Kyttaris VC, Juang YT, Tsokos GC. Protein phosphatase 2A is a negative regulator of IL-2 production in patients with systemic lupus erythematosus. J Clin Invest. 2005; 115(11):3193–3204. [PubMed: 16224536]
12. Xie L, et al. Protein phosphatase 2A catalytic subunit alpha plays a MyD88-dependent, central role in the gene-specific regulation of endotoxin tolerance. Cell Rep. 2013; 3(3):678–688. [PubMed: 23434512]
13. Zhou P, et al. In vivo discovery of immunotherapy targets in the tumour microenvironment. Nature. 2014; 506(7486):52–57. [PubMed: 24476824]
14. Long L, et al. Recruitment of phosphatase PP2A by RACK1 adaptor protein deactivates transcription factor IRF3 and limits type I interferon signaling. Immunity. 2014; 40(4):515–529. [PubMed: 24726876]
15. Stritesky GL, Jameson SC, Hogquist KA. Selection of self-reactive T cells in the thymus. Annu Rev Immunol. 2012; 30:95–114. [PubMed: 22149933]
16. Levine AG, Arvey A, Jin W, Rudensky AY. Continuous requirement for the TCR in regulatory T cell function. Nat Immunol. 2014; 15(11):1070–1078. [PubMed: 25263123]
17. Salomon B, et al. B7/CD28 costimulation is essential for the homeostasis of the CD4+CD25+ immunoregulatory T cells that control autoimmune diabetes. Immunity. 2000; 12(4):431–440. [PubMed: 10795741]
18. Fontenot JD, Rasmussen JP, Gavin MA, Rudensky AY. A function for interleukin 2 in Foxp3-expressing regulatory T cells. Nat Immunol. 2005; 6(11):1142–1151. [PubMed: 16227984]
19. Setoguchi R, Hori S, Takahashi T, Sakaguchi S. Homeostatic maintenance of natural Foxp3(+) CD25(+) CD4(+) regulatory T cells by interleukin (IL)-2 and induction of autoimmune disease by IL-2 neutralization. J Exp Med. 2005; 201(5):723–735. [PubMed: 15753206]
20. Delgoffe GM, et al. The kinase mTOR regulates the differentiation of helper T cells through the selective activation of signaling by mTORC1 and mTORC2. Nat Immunol. 2011; 12(4):295–303. [PubMed: 21358638]
21. Haxhinasto S, Mathis D, Benoist C. The AKT-mTOR axis regulates de novo differentiation of CD4+Foxp3+ cells. J Exp Med. 2008; 205(3):565–574. [PubMed: 18283119]
22. Shrestha S, et al. Treg cells require the phosphatase PTEN to restrain TH1 and TFH cell responses. Nat Immunol. 2015; 16(2):178–187. [PubMed: 25559258]
23. Delgoffe GM, et al. Stability and function of regulatory T cells is maintained by a neuropilin-1-semaphorin-4a axis. Nature. 2013; 501(7466):252–256. [PubMed: 23913274]
24. Hombauer H, et al. Generation of active protein phosphatase 2A is coupled to holoenzyme assembly. PLoS Biol. 2007; 5(6):e155. [PubMed: 17550305]
25. Sents W, Ivanova E, Lambrecht C, Haesen D, Janssens V. The biogenesis of active protein phosphatase 2A holoenzymes: a tightly regulated process creating phosphatase specificity. FEBS J. 2013; 280(2):644–661. [PubMed: 22443683]
26. Jiang L, et al. Structural basis of protein phosphatase 2A stable latency. Nat Commun. 2013; 4:1699. [PubMed: 23591866]
27. Haesen D, Sents W, Lemaire K, Hoorne Y, Janssens V. The Basic Biology of PP2A in Hematologic Cells and Malignancies. Front Oncol. 2014; 4:347. [PubMed: 25566494]
28. Brunkow ME, et al. Disruption of a new forkhead/winged-helix protein, scurfin, results in the fatal lymphoproliferative disorder of the scurfy mouse. Nat Genet. 2001; 27(1):68–73. [PubMed: 11138001]

29. Baharians Z, Schonthal AH. Autoregulation of protein phosphatase type 2A expression. J Biol Chem. 1998; 273(30):19019–19024. [PubMed: 9668082]
30. Janssens V, Longin S, Goris J. PP2A holoenzyme assembly: in cauda venenum (the sting is in the tail). Trends Biochem Sci. 2008; 33(3):113–121. [PubMed: 18291659]
31. Chen J, Martin BL, Brautigan DL. Regulation of protein serine-threonine phosphatase type-2A by tyrosine phosphorylation. Science. 1992; 257(5074):1261–1264. [PubMed: 1325671]
32. Neviani P, et al. The tumor suppressor PP2A is functionally inactivated in blast crisis CML through the inhibitory activity of the BCR/ABL-regulated SET protein. Cancer Cell. 2005; 8(5):355–368. [PubMed: 16286244]
33. Trotta R, et al. The PP2A inhibitor SET regulates natural killer cell IFN-gamma production. J Exp Med. 2007; 204(10):2397–2405. [PubMed: 17875674]
34. Li M, Makkinje A, Damuni Z. The myeloid leukemia-associated protein SET is a potent inhibitor of protein phosphatase 2A. J Biol Chem. 1996; 271(19):11059–11062. [PubMed: 8626647]
35. Dobrowsky RT, Kamibayashi C, Mumby MC, Hannun YA. Ceramide activates heterotrimeric protein phosphatase 2A. J Biol Chem. 1993; 268(21):15523–15530. [PubMed: 8393446]
36. Oaks J, Ogretmen B. Regulation of PP2A by Sphingolipid Metabolism and Signaling. Front Oncol. 2014; 4:388. [PubMed: 25642418]
37. Mukhopadhyay A, et al. Direct interaction between the inhibitor 2 and ceramide via sphingolipid-protein binding is involved in the regulation of protein phosphatase 2A activity and signaling. FASEB J. 2009; 23(3):751–763. [PubMed: 19028839]
38. Feuerer M, Hill JA, Mathis D, Benoist C. Foxp3+ regulatory T cells: differentiation, specification, subphenotypes. Nat Immunol. 2009; 10(7):689–695. [PubMed: 19536194]
39. Luberto C, Hannun YA. Sphingomyelin synthase, a potential regulator of intracellular levels of ceramide and diacylglycerol during SV40 transformation. Does sphingomyelin synthase account for the putative phosphatidylcholine-specific phospholipase C? J Biol Chem. 1998; 273(23): 14550–14559. [PubMed: 9603970]
40. Separovic D, et al. Sphingomyelin synthase 1 suppresses ceramide production and apoptosis post-photodamage. Biochem Biophys Res Commun. 2007; 358(1):196–202. [PubMed: 17467659]
41. Arvey A, et al. Inflammation-induced repression of chromatin bound by the transcription factor Foxp3 in regulatory T cells. Nat Immunol. 2014; 15(6):580–587. [PubMed: 24728351]
42. Laplante M, Sabatini DM. mTOR signaling in growth control and disease. Cell. 2012; 149(2):274–293. [PubMed: 22500797]
43. Zeng H, et al. mTORC1 couples immune signals and metabolic programming to establish T(reg)-cell function. Nature. 2013; 499(7459):485–490. [PubMed: 23812589]
44. Marin TM, et al. Rapamycin reverses hypertrophic cardiomyopathy in a mouse model of LEOPARD syndrome-associated PTPN11 mutation. J Clin Invest. 2011; 121(3):1026–1043. [PubMed: 21339643]
45. Liu G, Yang K, Burns S, Shrestha S, Chi H. The S1P(1)-mTOR axis directs the reciprocal differentiation of T(H)1 and T(reg) cells. Nat Immunol. 2010; 11(11):1047–1056. [PubMed: 20852647]
46. Battaglia M, Stabilini A, Roncarolo MG. Rapamycin selectively expands CD4+CD25+FoxP3+ regulatory T cells. Blood. 2005; 105(12):4743–4748. [PubMed: 15746082]
47. Samstein RM, et al. Foxp3 exploits a pre-existent enhancer landscape for regulatory T cell lineage specification. Cell. 2012; 151(1):153–166. [PubMed: 23021222]
48. Maceyka M, Spiegel S. Sphingolipid metabolites in inflammatory disease. Nature. 2014; 510(7503):58–67. [PubMed: 24899305]
49. Andjelkovic M, et al. Activation and phosphorylation of a pleckstrin homology domain containing protein kinase (RAC-PK/PKB) promoted by serum and protein phosphatase inhibitors. Proc Natl Acad Sci U S A. 1996; 93(12):5699–5704. [PubMed: 8650155]
50. Huynh A, et al. Control of PI(3) kinase in Treg cells maintains homeostasis and lineage stability. Nat Immunol. 2015; 16(2):188–196. [PubMed: 25559257]

51. Ruediger R, Ruiz J, Walter G. Human cancer-associated mutations in the Aalpha subunit of protein phosphatase 2A increase lung cancer incidence in Aalpha knock-in and knockout mice. Mol Cell Biol. 2011; 31(18):3832–3844. [PubMed: 21791616]

52. Rubtsov YP, et al. Regulatory T cell-derived interleukin-10 limits inflammation at environmental interfaces. Immunity. 2008; 28(4):546–558. [PubMed: 18387831]

53. Bielawski J, et al. Comprehensive quantitative analysis of bioactive sphingolipids by high-performance liquid chromatography-tandem mass spectrometry. Methods Mol Biol. 2009; 579:443–467. [PubMed: 19763489]

54. Wu Y, et al. FOXP3 controls regulatory T cell function through cooperation with NFAT. Cell. 2006; 126(2):375–387. [PubMed: 16873067]

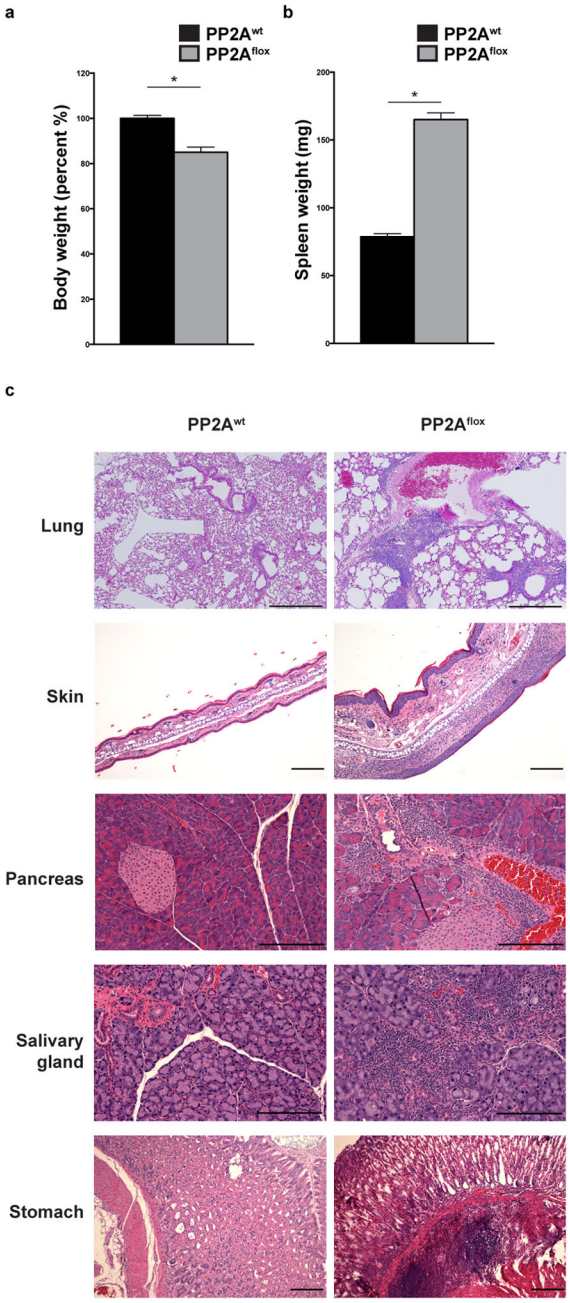

Figure 1. PP2A^{flox} mice develop multi-organ autoimmunity

(**a, b**) The body weight (a, n=17 for PP2A^{wt} and n=9 for PP2A^{flox}) and the spleen weight (b, n=5 per group) of 10–14 week-old PP2A^{wt} and PP2A^{flox} mice were quantified. (**c**) H&E staining of the lungs, the skin, the pancreas, the salivary glands and the stomach of PP2A^{wt} and PP2A^{flox} mice (scale bar represents 200 μm). Images are from one experiment representative of three independent experiments with similar results (n=3 mice per group per experiment). Mean ± s.e.m. is shown, *P<0.001 (unpaired, two-tailed t-test).

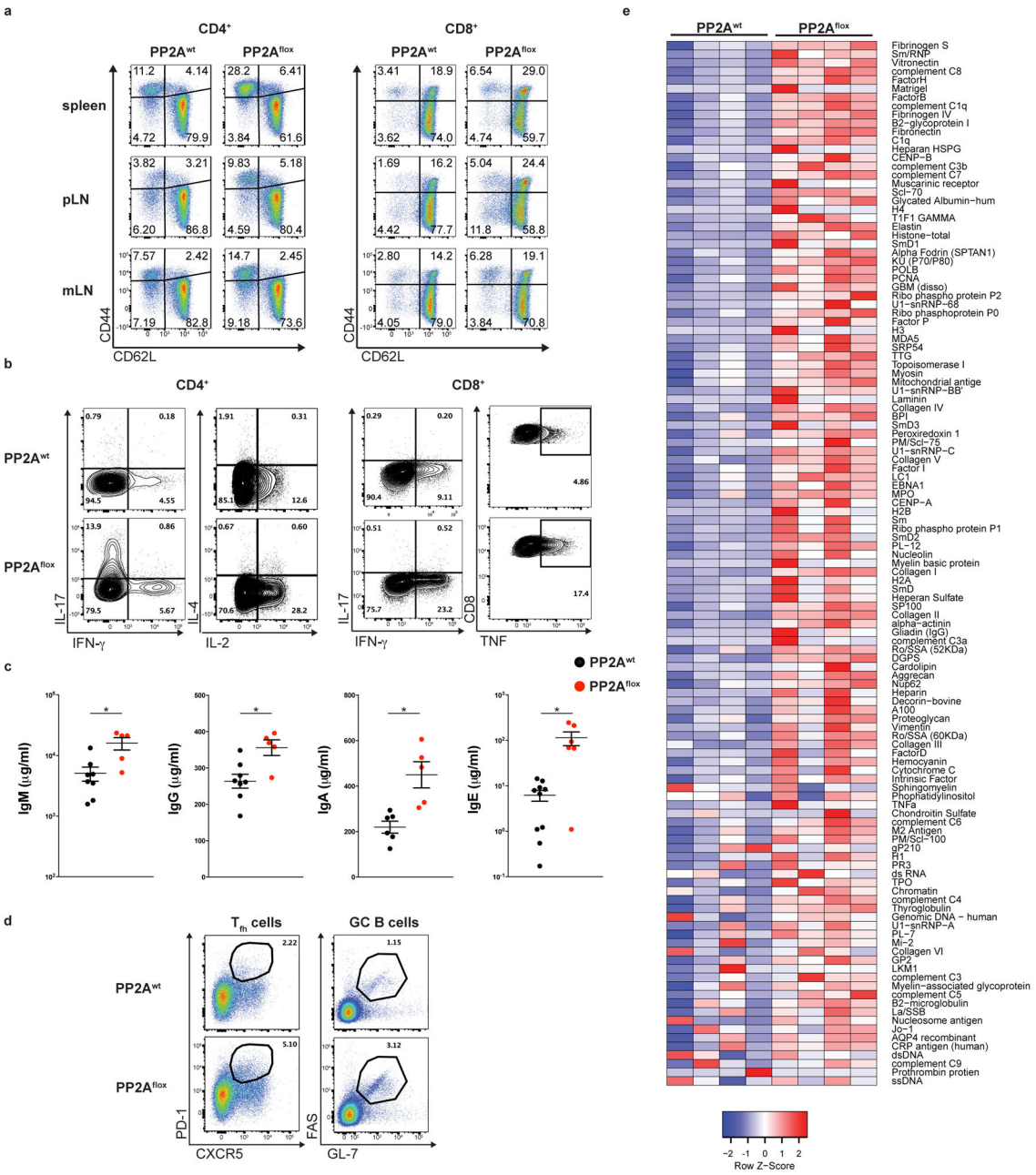

Figure 2. Spontaneous T cell and B cell activation in PP2A^{flox} mice

(**a, b**) CD4$^+$ and CD8$^+$ T cells of 10–14 week-old PP2A^{wt} and PP2A^{flox} mice were stained for CD62L and CD44 (a, spleen, peripheral and mesenteric lymph nodes) and for the production of the indicated cytokines (b, spleen). Data shown are from one experiment representative of three independent experiments (n=3 mice per group) (**c**) The levels of serum IgM, IgG, IgA and IgE in PP2A^{wt} and PP2A^{flox} mice were quantified (n=8 for PP2A^{wt} and n=5 for PP2A^{flox} mice). (**d**) The percentages of T follicular helper (T_{fh}) cells and germinal center (GC) B cells in the spleen from PP2A^{wt} and PP2A^{flox} mice are shown. Data shown are from one experiment representative of two independent experiments (n=3

mice per group per experiment). **(e)** Sera from $PP2A^{wt}$ and $PP2A^{flox}$ mice were analyzed for the presence of autoantibodies. Each individual column of the heatmap represents an individual mouse (total 4 mice per group). Mean ± s.e.m is shown. *P<0.01 (unpaired, two-tailed t-test).

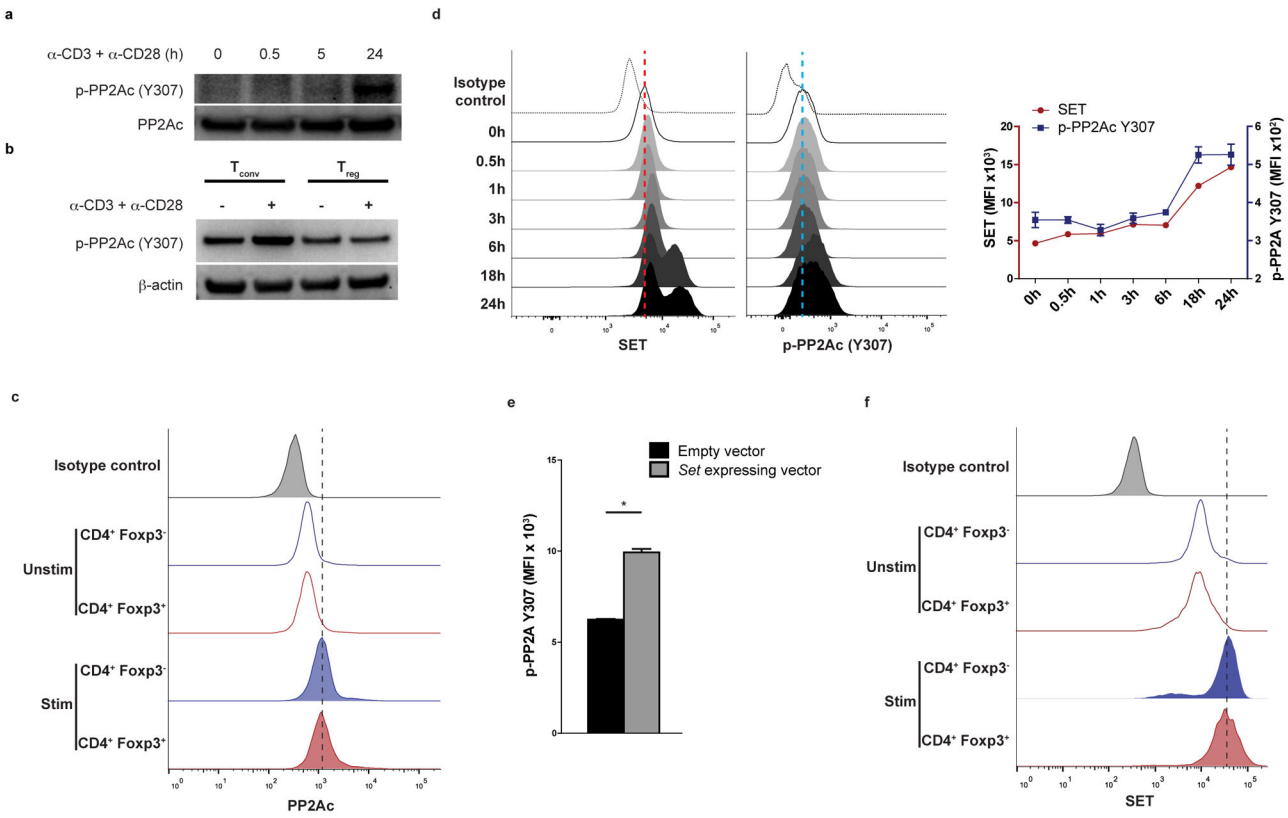

Figure 3. TCR activation induces SET-mediated phosphorylation of PP2A$_C$ at Y307 in T$_{conv}$ cells but not T$_{reg}$ cells

(**a, b**) Naïve CD4$^+$ T cells (a) or T$_{conv}$ and T$_{reg}$ cells (b) were stimulated with CD3 plus CD28 antibodies for the indicated time periods. Immunoblotting for p-PP2A$_C$ (Y307) was then performed. Data are from one experiment representative of two independent experiments with similar results (n=3 mice per experiment). (**c, f**) Splenocytes isolated from Foxp3$^{IRES-GFP}$ mice were stimulated with CD3 plus CD28 antibodies for 24 hours or left unstimulated. Intracellular staining was then performed for PP2A$_C$ (c) or SET (f). Data are from one experiment representative of three independent experiments with similar results (n=3 mice per experiment). (**d**) Naïve CD4$^+$ T cells were stimulated with CD3 plus CD28 for 0, 0.5, 1, 3, 6, 18 and 24 hours. Intracellular staining was then performed for SET and p-PP2A$_C$ (Y307). A representative histogram (left) and quantification of the results (right) is shown from one of two independent experiments with similar results (n=3 per group). (**e**) Intracellular staining for p-PP2A$_C$ (Y307) of naïve CD4$^+$ T cells activated with CD3 plus CD28 antibodies for 24 hours and then spin-infected with an empty or a *Set*-expressing mCherry lentiviral vector. The analysis was done on mCherry$^+$ T cells (n=5 per group, one of two experiments with similar results is shown). Mean ± s.e.m. is shown, MFI: Mean fluorescent intensity, **P*<0.01 (unpaired, two-tailed t-test).

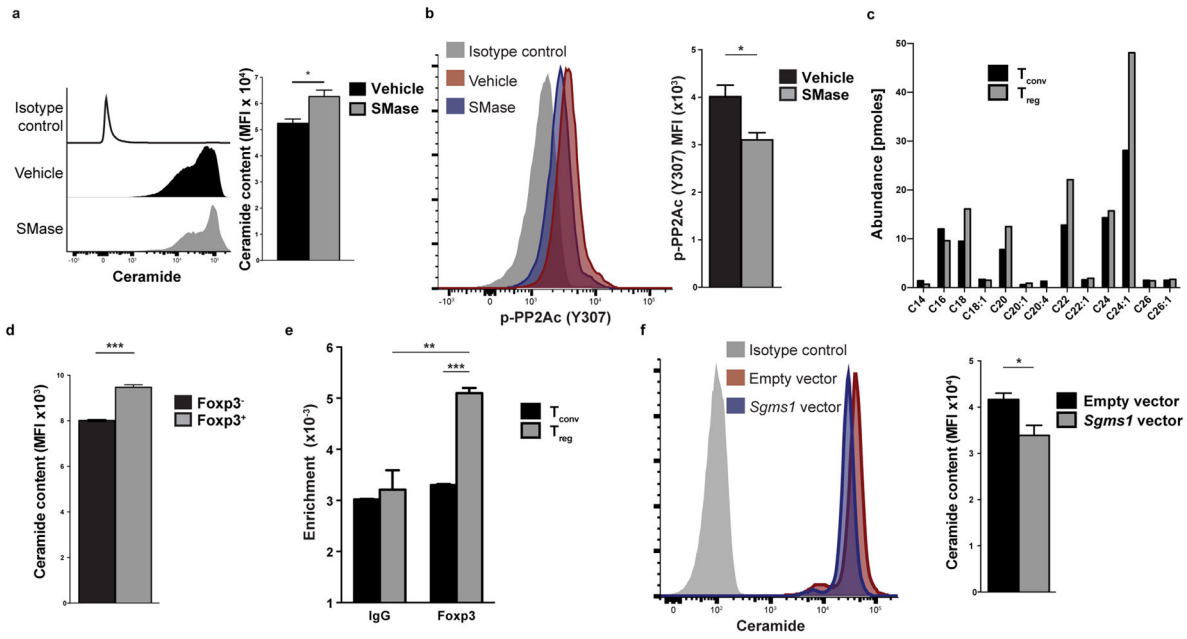

Figure 4. T_{reg} cells display higher ceramide content through Foxp3-mediated inhibition of *Sgms1*

(**a, b**) Naïve $CD4^+$ T cells were stimulated with anti-CD3 plus anti-CD28 for 24h and then treated with sphingomyelinase (SMase, 0.5 units/mL) or vehicle (50% glycerol in PBS) for 1h. The cells were then stained for ceramide (a) or p-$PP2A_C$ (Y307) (b). A representative histogram (left) and quantification of the results (right) is shown (n=3, one of two experiments with similar results is shown). (**c**) T_{conv} and T_{reg} cells were stimulated for 24h and then subjected to ESI-MS/MS for the quantification of ceramide species. (**d**) Ceramide content of $CD3^+CD4^+Foxp3^-$ and $CD3^+CD4^+Foxp3^+$ was quantified using flow cytometry (n=3 mice). Data are from one of three experiments with similar results. (**e**) T_{conv} and T_{reg} cells were subjected to chromatin immunoprecipitation using a Foxp3-specific antibody or an IgG control antibody. Shown is binding enrichment at the mouse *Sgms1* gene, normalized to the input (n=3 per group, one representative of two independent experiments with similar results is shown). (**f**) Naïve $CD4^+$ T cells were stimulated for 24h and then spin-infected with an mCherry-expressing lentivirus that harbored or not the murine *Sgms1* coding sequence. $CD4^+mCherry^+$ cells were analyzed for ceramide content using flow cytometry. A representative histogram (left) and quantification of the results (right) is shown. Data are from one experiment representative of two independent experiments with similar results. Mean ± s.e.m. is shown, MFI: Mean fluorescent intensity, $*P<0.05$, $**P<0.01$, $***P<0.001$ (unpaired, two-tailed t-test).

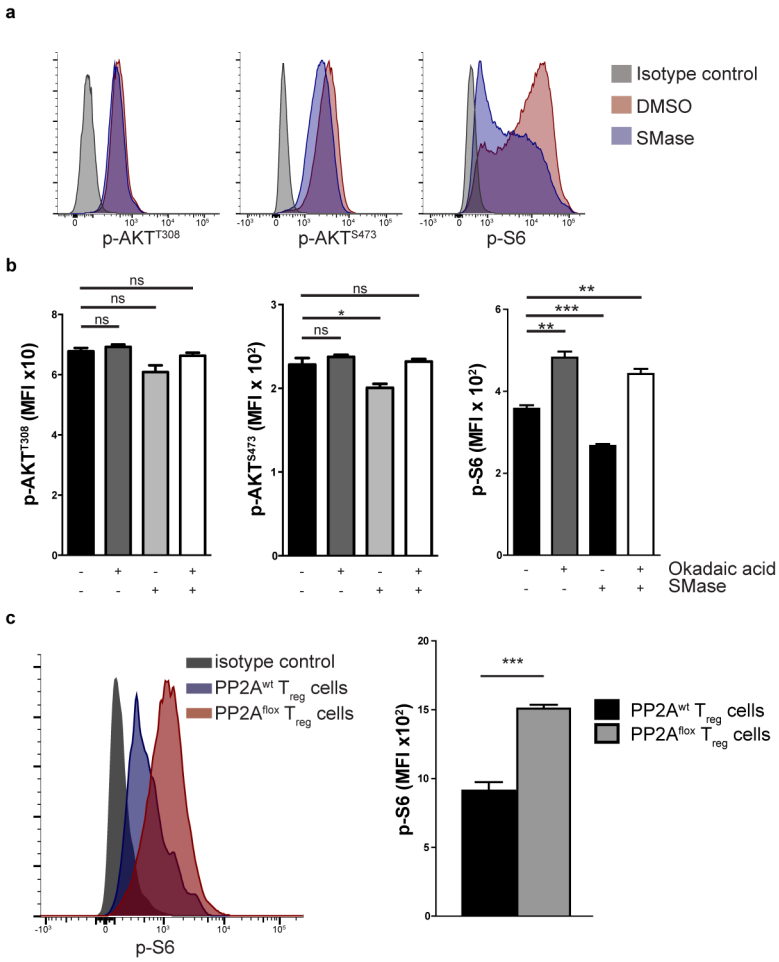

Figure 5. PP2A inhibits the mTORC1 pathway in T_{reg} cells

(a) Jurkat T cells were treated with SMase (0.5 units/mL) or vehicle (50% glycerol in PBS) for 1 hour and then stained for p-AKT^{T308}, p-AKT^{S473} and p-S6. Data are from one experiment representative of two independent experiments with similar results. (**b**) Naïve CD4$^+$ T cells were stimulated with CD3 plus CD28 antibodies (2 μg/mL) for 24h and then incubated with okadaic acid or DMSO for 3 hours. During the last hour the cells were treated with SMase or vehicle and then stained for p-AKT^{T308}, p-AKT^{S473} and p-S6 (n=3 per treatment group). Data are from one experiment representative of two independent experiments with similar results. (**c**) Foxp3$^+$ T_{reg} cells were isolated from PP2A^{wt} and PP2A^{flox} mice and stained for p-S6 (n=3 mice per group). A representative histogram (left) and quantification of the results (right) is shown. Data are from one experiment representative of three independent experiments with similar results. Mean ± s.e.m., MFI: Mean fluorescent intensity, ns $P>0.05$, *$P<0.05$, **$P<0.01$, ***$P<0.001$ (unpaired, two-tailed t-test).

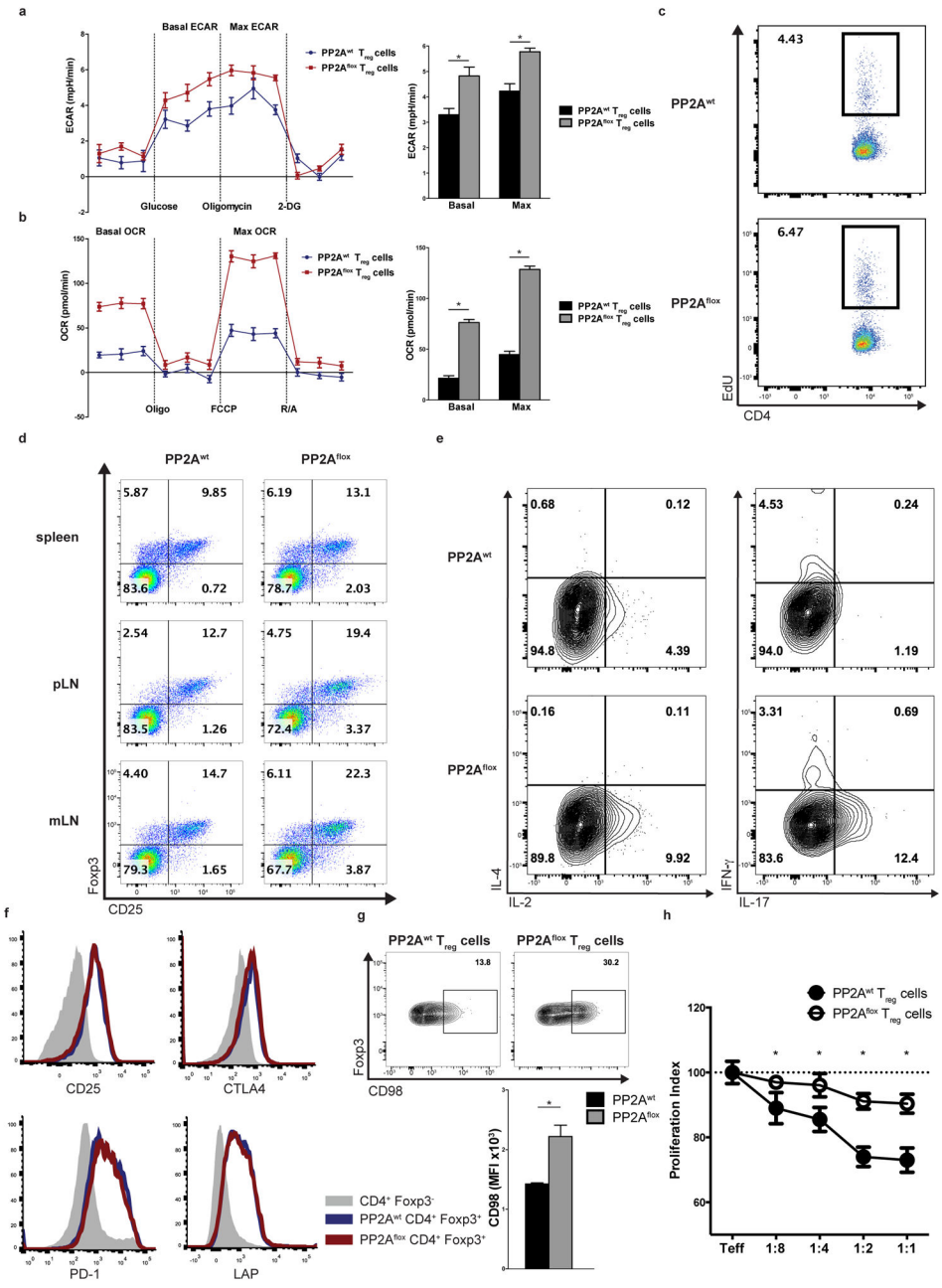

Figure 6. PP2A^{flox} T$_{regs}$ exhibit metabolic, proliferation and cytokine production abnormalities

(**a, b**) The extracellular acidification rate (a, ECAR) and the oxygen consumption rate (b, OCR) of PP2A^{wt} and PP2A^{flox} T$_{reg}$ cells are shown. *Left:* Representative stress tests (a: glycostress test, b: mitostress test). *Right*: quantification of the results is shown (n=4). Data are from one experiment representative of three independent experiments with similar results. (**c**) The proliferation rate of PP2A^{wt} and PP2A^{flox} T$_{reg}$ cells was quantified *in vivo* after i.p. injection of EdU (n=3, one experiment is shown representative of two independent experiments). (**d**) The percentage of CD25^{+}Foxp3-YFP^{+} T cells in the spleens, peripheral and mesenteric lymph nodes of 10–14 week-old PP2A^{wt} and PP2A^{flox} mice is shown (n=4

mice per group, one experiment is shown representative of two independent experiments). (**e**) T_{reg} cells from the spleens of 10–14 week-old $PP2A^{wt}$ and $PP2A^{flox}$ mice were stimulated with PMA/Ionomycin for 6h and then stained intracellularly for the indicated cytokines (n=3 mice per group). Data are from one experiment representative of three independent experiments with similar results. **(f, g)** $PP2A^{wt}$ and $PP2A^{flox}$ T_{reg} cells were stained for CD25, CTLA-4, PD-1 and LAP (f) or CD98 (g, representative histogram and quantification of the results is shown). Data are from one experiment representative of two independent experiments with similar results (n=3 mice per group) **(h)** *In vitro* suppression assay using effector $CD45.1^{+}CD4^{+}$ (T_{eff}) T cells and $PP2A^{wt}$ or $PP2A^{flox}$ T_{reg} cells at the indicated ratios (T_{eff}:T_{reg} cells). Mean ± s.e.m., MFI: Mean fluorescent intensity, *P<0.001 (unpaired, two-tailed t-test).

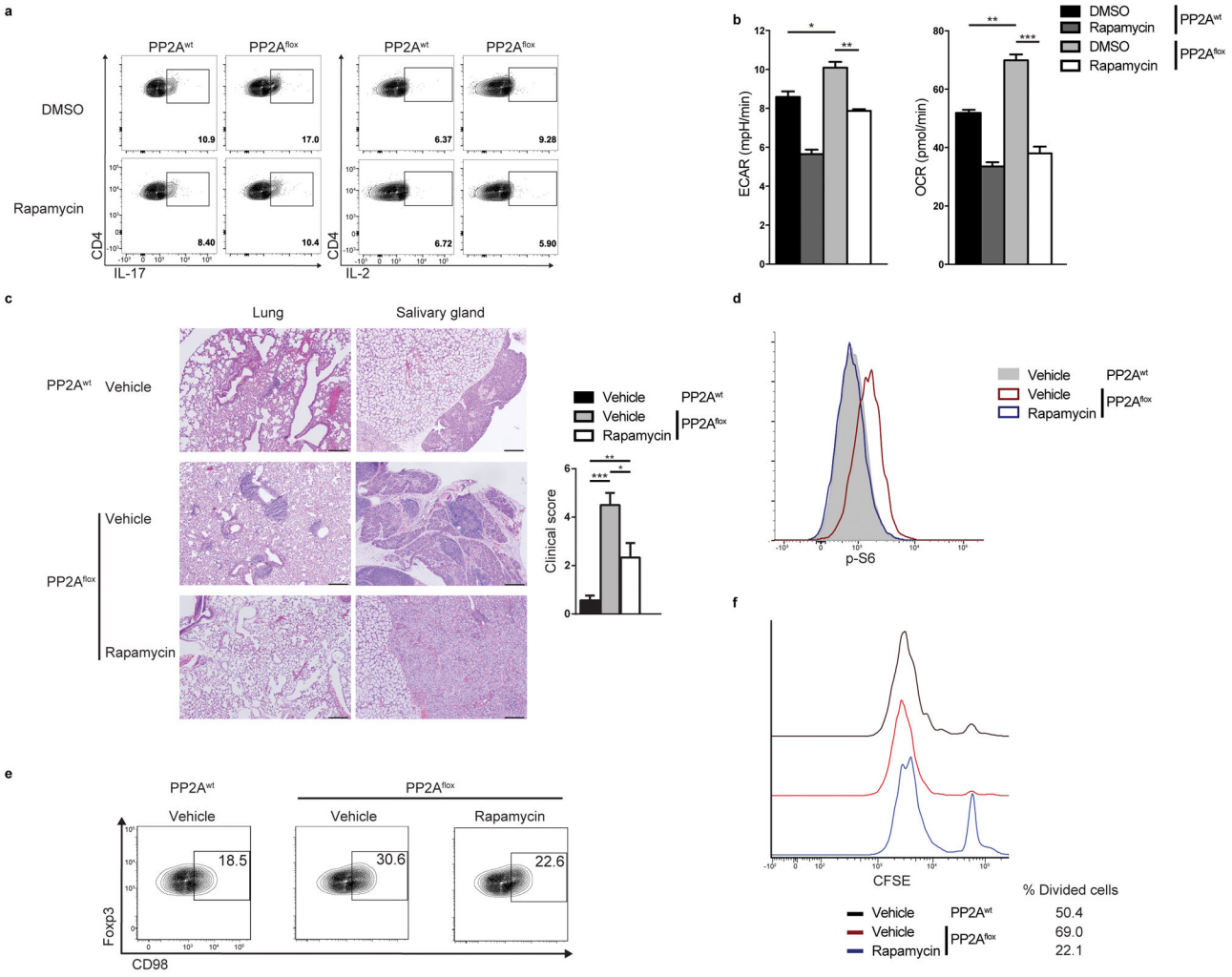

Figure 7. Rapamycin reverses the abnormal profile of the PP2A^{flox} T$_{reg}$ cells

(**a, b**) FACS-sorted PP2A^{wt} and PP2A^{flox} T$_{reg}$ cells were stimulated with CD3 plus CD28 and then expanded for 4 days in the presence of 100 IU/mL of IL-2. During the final 24 hours, they were treated with 100nM of Rapamycin or DMSO. (a) The T$_{reg}$ cells (gated on FoxP3-YFP^{+}CD4^{+} T cells) were re-stimulated with PMA/Ionomycin for 6 hours and stained for IL-17 and IL-2. (b) The ECAR and OCR of PP2A^{wt} and PP2A^{flox} T$_{reg}$ cells (sorted again as Foxp3-YFP^{+}CD4^{+} T cells at the end of the culture) were measured (n=3 mice per group, unpaired, two-tailed t-test). Data are from one experiment representative of two independent experiments with similar results. (**c**) *Left*: H&E staining of the lungs and the salivary glands of PP2A^{wt} and PP2A^{flox} mice treated or not with rapamycin (scale bar represents 100 μm). Images are from one experiment representative of two independent experiments with similar results. *Right*: combined clinical score of inflammation in the liver, skin, stomach, salivary glands, lungs and pancreas of PP2A^{wt} and PP2A^{flox} mice treated or not with rapamycin (one-way analysis of variance (ANOVA) followed by Tukey's multiple comparison test). (**d, e**) *Ex vivo* amounts of p-S6 (d) and CD98 expression (e) in T$_{regs}$ (FoxP3-YFP^{+}) from mice in (c). **(f)** *In vitro* suppression assay using effector CD45.1^{+}CD4^{+}

(T_{eff}) T cells and T_{reg} cells from $PP2A^{wt}$ or $PP2A^{flox}$ rapamycin-treated and vehicle-treated mice. Representative histograms showing CFSE dilution and percentage of divided cells (ratio T_{reg}/T_{eff}: 1/1). Data are from one experiment representative of two independent experiments with similar results. Mean ± s.e.m., *P<0.05, **P<0.01, ***P<0.001.